Efficient coupling between a photonic crystal nanocavity and a waveguide with directional end-facet emission

Ling Lu[1], Adam Mock[2] and John O'Brien

Department of Electrical Engineering, University of Southern California, Los Angeles, CA 90089, USA

E-mail: linglu@mit.edu

Abstract
Monolithic integration of photonic crystal lasers and waveguides is proposed using quantum well intermixing. Coupling between a double-heterostructure nanocavity and a regular single-line-defect waveguide is optimized to have a high coupling efficiency (93%) and a high quality factor (6.8×10^3) without fine-tuning of the lattice. The design is completed with a waveguide exit of robust directional far-field. All calculations were performed using the three-dimensional finite-difference time-domain method.

Keywords: monolithic integration, nanocavity laser, cavity waveguide coupling, directional facet emission, photonic crystal, quantum well intermixing

(Some figures may appear in colour only in the online journal)

Two-dimensional slab photonic crystals (PhCs) are popular planar platforms of miniature optical circuits for classical and quantum communications. A cavity and a waveguide are two important device elements on chip; they (in PhCs) both have advantages over their conventional counterparts and a large degree of freedom which can lead to unprecedented performance after optimization. A PhC defect cavity offers a single high quality factor (Q) mode of small mode volume. Such a resonator is suitable for on-chip sources like low-threshold nanocavity lasers [1] and efficient single-photon emitters [2]. PhC defect waveguides can bend sharp corners [3] and slow light down with large group velocities [4]. Interfacing them requires efficient coupling between the active cavity and passive waveguide monolithically.

Several studies have been done on the nanocavity–waveguide coupling in membrane triangular lattice 2D PhCs to achieve high coupling efficiencies and high cavity Qs. Kim *et al* [5] compared different coupling geometries between a single-cell defect cavity and a modified single-line-defect (W1) waveguide. They found the spatial overlap between the cavity mode profile and the waveguide is an important criterion for efficient coupling. Faraon *et al* [6] optimized the coupling between an L3 cavity and a modified W1 waveguide. The cavity Q of 500 and 90% coupling efficiency were obtained. Nozaki *et al* [7] reported a cavity Q of 10^3 and a coupling efficiency of 80% between an H0 cavity and a modified W1 waveguide. In order to match the frequencies of the cavity and the waveguide, one of them has to be modified. Although tuning of the local cavities is preferred to match a common waveguide, the cavity geometries in the above demonstrations are not easily tailored without scarifying their performances or complicating the fabrication. So the W1 waveguides were modified by altering the innermost air-hole size or waveguide width. In addition, no output solutions for the waveguides were provided.

Our design differs from the above results in the following ways. First, we optimized the coupling between a double-heterostructure (DH) cavity [8] and a regular W1 waveguide. Without changing its Q and mode profile, the DH cavity frequency can be smoothly tuned to match the waveguide dispersion by varying the cavity width (w in
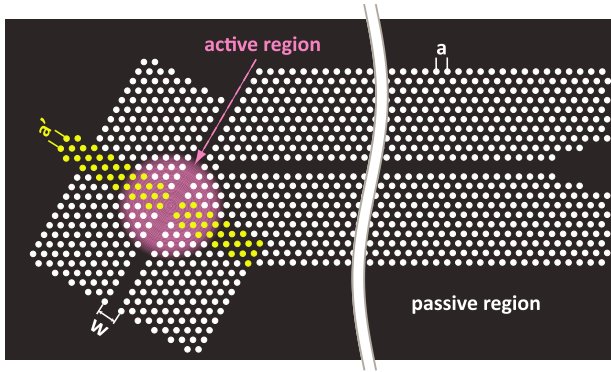

1

Figure 1. Schematics of a PhC DH cavity coupled to an adjacent waveguide. The DH cavity is 60° tilted from the horizontal extraction waveguide to optimize the coupling between the DH cavity and the W1 waveguide. The perturbed lattice with lattice constant (a') is in yellow and the rest of the PhCs have a lattice constant of a, which is 5% smaller than a'. The waveguide exit is enlarged to have a directional far-field emission. This configuration corresponds to coupling position 4 in the later discussion. The radius over lattice constant ratio is the same everywhere.
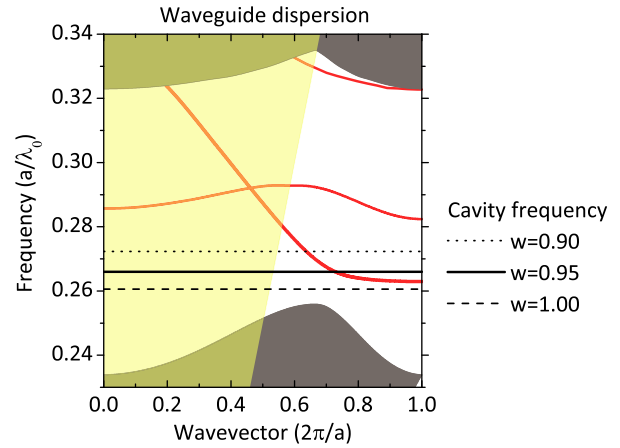

Figure 2. Dispersion relation of a regular W1 PhC waveguide. The resonant frequencies of the DH nanocavity with different defect waveguide width (w) are plotted as lines. The waveguide modes are plotted in red. The filled gray area represents PhC cladding modes. The transparent yellow area is the light cone.

figure 1). This preserves the lattice symmetry and makes the fabrication easier. Second, our optimized design provides high Q (well above 10^3) and high coupling efficiency (>90%) at the same time, which was not realized in the previous efforts. Last, but not least, we also provide a waveguide out-coupling solution to complete this study, so the optical power inside the waveguide can be well collected in free space. Furthermore, the directional emission is not sensitive to the waveguide termination; it is robust against fabrication error.

In order to have the most efficient cavity–waveguide coupling, one wants to start with a cavity with a Q as high as possible, then increase the optical loss by channeling all the optical power into the adjacent waveguide. PhC DH nanocavity [9] is thus the choice. Using this DH membrane cavity, we have demonstrated high peak power edge-emitting lasers [10–12] and improvement in laser performance by removing the optical absorption loss using quantum well intermixing (QWI) [13]. QWI is a much simpler monolithic integration platform [14] for PhC nanocavity lasers over the previously used regrowth approaches [7, 15, 16]. The regrowth method suffers from difficulties in the second growth such as abrupt hetero-interfaces and low spatial resolution. Figure 1 illustrates the proposed integration scheme. The gain region containing original QWs covers the center of the cavity, where the high-Q mode is confined, to supply optical gain. The QWs in the rest of the area are intermixed and passive.

The cavity–waveguide coupling occurs in both frequency and space. Figure 2 plots the frequency lineup between the DH cavity and the W1 waveguide. A regular DH cavity, $w = 1.00(\sqrt{3}a)$, has its high-Q resonant mode frequency bounded just below the band edge of the waveguide dispersion [17], thus the coupling will not happen. Squeezing the cavity width (w) pushes the resonant frequency up into the guiding band of the waveguide. This slight change in w does not alter the Q or mode profile of the cavity. When $w = 0.90(\sqrt{3}a)$, the coupling happens at the linear range of the

waveguide dispersion. In this design, we set the width to be $w = 0.95(\sqrt{3}a)$ so that the far-field from the waveguide exit is highly directional, which is desired for free space detection. This flexible frequency-tuning of the DH cavity is an advantage over other nanocavities.

Parallelized self-written three-dimensional finite-difference time-domain (3D FDTD) code [18] was used to perform the calculations. The PhC semiconductor membrane (refractive index of 3.4) of thickness $0.6a$ is surrounded by air. The radius over lattice constant ratio is fixed at 0.3 for all air holes in the membrane. The calculation domain is terminated by perfect matched layers (PML). Padé interpolation of the Fourier-transformed time-domain signals is used to extract the quality factors of the passive resonators. Optical power is calculated by time-averaging Poynting vectors. The cavity–waveguide coupling efficiency is evaluated by dividing the power exiting the waveguide by the total power exiting a closed box enclosing the cavity. The lens collection efficiency is defined by the fraction of total power goes into a conical area, set by the NA of a lens, from the center of the waveguide facet.

Spatial placement of the waveguide with respect to the cavity needs to be optimized for the coupling efficiency between them. The previous studies show that the optimal coupling takes place when the waveguide approaches the cavity in the direction where the cavity mode is mostly extended in space [6, 5, 7]. In figure 3, the DH mode profile is plotted on a log scale and nine candidate positions for the starting point of the waveguide are labeled. The coupling efficiencies and the corresponding Q values are plotted in figure 4. As the waveguide approaches the field maximum of the cavity mode, optical loss into the waveguide increases and the cavity Q decreases. The difficulty in the coupling design lies in the simultaneous realization of high cavity–waveguide coupling efficiency and high cavity Q values. Figure 4 shows high coupling efficiency (above 90%) and high cavity Q (well above 1000) for coupling position at 4–7. The cavity Q values
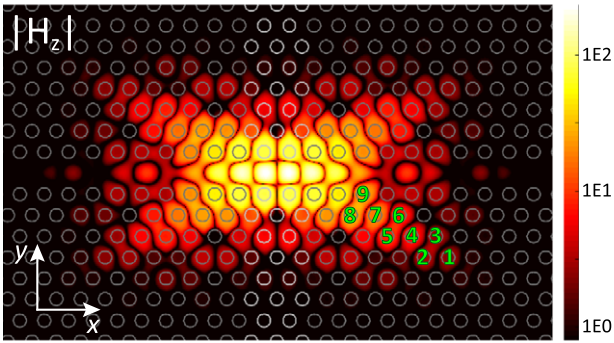
Figure 3. H_z field component of the DH mode at the center of the membrane. Nine different waveguide starting points are labeled from 1 to 9. The interfaces between semiconductor and air are outlined in gray. The central perturbed lattice (5% increase in lattice constant) is outlined in lighter gray.
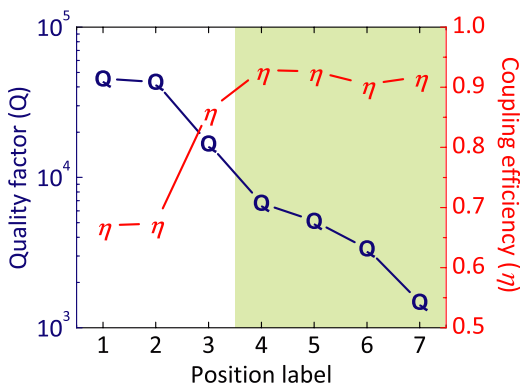

Figure 4. Results from 3D FDTD calculations of different cavity–waveguide coupling geometries. The Q factors of the DH mode and the coupling efficiencies into the waveguide are plotted versus waveguide starting positions. High performance designs are highlighted with green background.

Figure 5. H_z field profiles of the coupling configuration of position 5. (a) Field distribution in the x–y plane at the center of the membrane. (b) Field distribution in the x–z plane through the waveguide center. The interfaces between semiconductor and air are outlined in gray. The central perturbed lattice (5% increase) region is outlined in lighter gray. It is worth pointing out that the two extra small air holes in the cavity are to suppress the side modes as discussed in detail in [18]. They do not affect other properties in this design. The waveguide length in the calculation is only limited by computing power.

of positions 8 and 9 are below 1000. The best coupling happens at positions 4 and 5; they both have high coupling efficiency of 92.9% and 92.6% and high cavity Q of 6.76×10^3 and 5.13×10^3, respectively. Figure 1 illustrates the coupling geometry of position 4. Field profile of coupling position 5 is plotted in figure 5. The performance of our design surpasses the previously reported ones and can still be improved by a more detailed engineering of the joint region between the cavity and waveguide.

Due to the sub-wavelength confinement of the PhC membrane waveguide, the field exiting the waveguide termination usually diffracts in large angles and is hard to collect. Directional emission out of a PhC waveguide has recently been subjected to heavy investigation, which is very important for in-and-out coupling of PhC devices. Taking advantage of the surface modes at waveguide termination is an interesting approach to obtain a far-field of low divergence, but this approach works in a very narrow bandwidth and is extremely sensitive to the surface termination [19, 20]. Kurt [21], according to his 2D simulations, suggested that directional emission of much larger bandwidth can be achieved by simply enlarging the waveguide exit. We verified,
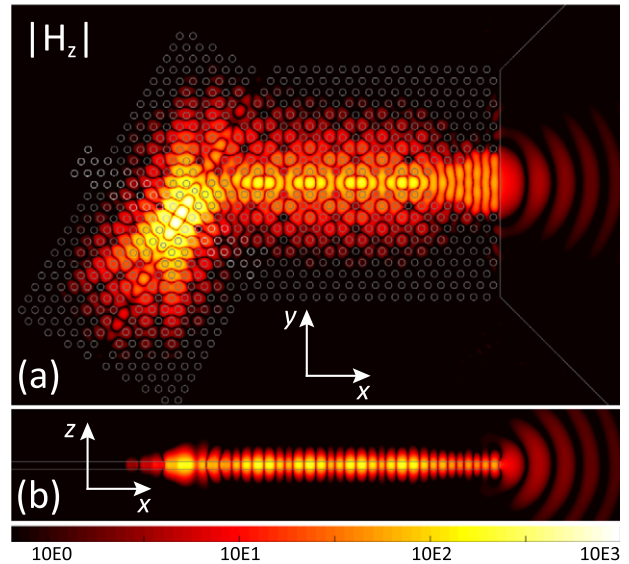
using 3D FDTD, that this approach can work for membrane structures. The specific design of the waveguide exit and the corresponding cavity frequency are optimized for our system. The result, shown in figure 5, is robust against facet termination (the location of termination in the unit cell); this is highly favorable for experimental realization due to fabrication uncertainties.

Figure 5 shows the field profile of the cavity–waveguide geometry of coupling position 5 with a directional far-field. Using a lens whose numerical aperture is 0.65, the coupling or collection efficiency from the cavity to the lens is about 38%. This is even higher than our best reported number in Ref. [12]. This number is bounded by the coupling efficiency between the cavity–waveguide and is solely limited by the diffraction in the direction perpendicular to the membrane as shown in figure 5(b).

In conclusion, we presented a complete and robust integration design of a PhC DH nanocavity laser and a single-line-defect waveguide with directional facet emission on an air-clad semiconductor slab. Record theoretical performances of 92.9% coupling efficiency and 6.76×10^3 cavity Q are achieved simultaneously. We believe this fabrication-friendly and ready-to-use design is beneficial to the integration of 2D PhC devices.

Acknowledgments

References

[1] Park H G, Kim S H, Kwon S H, Ju Y G, Yang J K, Baek J H, Kim S B and Lee Y H 2004 Electrically driven single-cell photonic crystal laser *Science* **305** 1444–7

[2] Chang W-H, Chen W-Y, Chang H-S, Hsieh T-P, Chyi J-I and Hsu T-M 2006 Efficient single-photon sources based on low-density quantum dots in photonic-crystal nanocavities *Phys. Rev. Lett.* **96** 117401

[3] Watanabe Y, Ikeda N, Sugimoto Y, Takata Y, Kitagawa Y, Mizutani A, Ozaki N and Asakawa K 2007 Topology optimization of waveguide bends with wide, flat bandwidth in air-bridge-type photonic crystal slabs *J. Appl. Phys.* **101** 113108

[4] Baba T 2008 Slow light in photonic crystals *Nature Photon* **2** 465–73

[5] Kim G H, Lee Y H, Shinya A and Notomi M 2004 Coupling of small, low-loss hexapole mode with photonic crystal slab waveguide mode *Opt. Express* **12** 6624–31

[6] Faraon A, Waks E, Englund D, Fushman I and Vuckovic J 2007 Efficient photonic crystal cavity–waveguide couplers *Appl. Phys. Lett.* **90** 073102

[7] Nozaki K, Watanabe H and Baba T 2008 Photonic crystal nanolaser monolithically integrated with passive waveguide for effective light extraction *Appl. Phys. Lett.* **92** 021108

[8] Song B S, Noda S, Asano T and Akahane Y 2005 Ultra-high-q photonic double-heterostructure nanocavity *Nature Mater.* **4** 207–10

[9] Tanaka Y, Asano T and Noda S 2008 Design of photonic crystal nanocavity With *Q*-Factor of ~10^9 *J. Lightwave Technol.* **26** 1532–9

[10] Yang T, Mock A, O'Brien J D, Lipson S and Deppe D G 2007 Edge-emitting photonic crystal double-heterostructure nanocavity lasers with inas quantum dot active material *Opt. Lett.* **32** 1153–5

[11] Lu L, Mock A, Yang T, Shih M H, Hwang E H, Bagheri M, Stapleton A, Farrell S, O'Brien J and Dapkus P D 2009 120 μw peak output power from edge-emitting photonic crystal double-heterostructure nanocavity lasers *Appl. Phys. Lett.* **94** 111101

[12] Lu L, Mock A, Hwang E H, O'Brien J and Dapkus P D 2009 High-peak-power efficient edge-emitting photonic crystal nanocavity lasers *Opt. Lett.* **34** 2646–8

[13] Lu L, Mock A, Bagheri M, Hwang E H, O'Brien J and Dapkus P D 2008 Double-heterostructure photonic crystal lasers with reduced threshold pump power and increased slope efficiency obtained by quantum well intermixing *Opt. Express* **16** 17342–7

[14] Skogen E J, Raring J W, Morrison G B, Wang C S, Lal V, Masanovic M L and Coldren L A 2005 Monolithically integrated active components: A quantum-well intermixing approach *IEEE J. Sel. Top. Quantum Electron.* **11** 343–55

[15] Watanabe H and Baba T 2008 High-efficiency photonic crystal microlaser integrated with a passive waveguide *Opt. Express* **16** 2694–8

[16] Matsuo S, Shinya A, Kakitsuka T, Nozaki K, Segawa T, Sato T, Kawaguchi Y and Notomi M 2010 High-speed ultracompact buried heterostructure photonic-crystal laser with 13 fJ of energy consumed per bit transmitted *Nature Photon* **4** 648–54

[17] Mock A, Lu L and O'Brien J D 2008 Spectral properties of photonic crystal double-heterostructure resonant cavities *Opt. Express* **16** 9391–7

[18] Mock A, Lu L, Hwang E H, O'Brien J and Dapkus P 2009 Modal analysis of photonic crystal double-heterostructure laser cavities *IEEE J. Sel. Top. Quantum Electron.* **15** 892–900

[19] Kramper P, Agio M, Soukoulis C M, Birner A, Muller F, Wehrspohn R B, Gosele U and Sandoghdar V 2004 Highly directional emission from photonic crystal waveguides of subwavelength width *Phys. Rev. Lett.* **92** 113903

[20] Moreno E, García-Vidal F J and Martín-Moreno L 2004 Enhanced transmission and beaming of light via photonic crystal surface modes *Phys. Rev.* B **69** 121402

[21] Kurt H 2009 The directional emission sensitivity of photonic crystal waveguides to air hole removal *Appl. Phys.* B **95** 341–4